Supplementary Information

On

Controllable Hydrogen-bonded Poly(dimethylsiloxane) (PDMS) Membranes for Ultrafast Alcohol Recovery

Tengyang Zhu[ab], Jiayu Dong[ab], Huan Liu[ab] and Yan Wang*[ab]

[1] *Key Laboratory of Material Chemistry for Energy Conversion and Storage (Huazhong University of Science and Technology), Ministry of Education, Wuhan, 430074, PR China*

[2] *Hubei Key Laboratory of Material Chemistry and Service Failure, School of Chemistry and Chemical Engineering, Huazhong University of Science & Technology, Wuhan, 430074, PR China*

* Corresponding author at: Key Laboratory of Material Chemistry for Energy Conversion and Storage (Huazhong University of Science & Technology), Ministry of Education, Wuhan, 430074, PR China

Tel.: 86 027-87543032; fax: 86 027-87543632.

E-mail address: wangyan@hust.edu.cn (Y. Wang)

The file includes:

Supplementary Text

Sections S1 to S23

Figs. S1 to S19

Tables S1 to S7

References (1 to 56)

S1. Materials employed in this work

bis(3-aminopropyl) terminated poly(dimethylsiloxane) (APDMS, M_n = 2.5 kDa) and silanol terminated poly(dimethylsiloxane) (HPDMS, M_n = 2.75 kDa) were purchased from Gelest. HPDMS (3000 cst, bought from Hubei Xin Si Hai Chemical Industry Co., Ltd.) was used to prepare covalently-crosslinked PDMS elastomer. Hexamethylene diisocyanate (HDI, 99%), 4,4'-diisocyanato-3,3'-dimethylbiphenyl (DDP, 98%), tetraethyl orthosilicate (TEOS, 98%), dibutyltin dilaurate (DBTDL, 95%), polyvinylpyrrolidone (PVP, M_n = 24 kDa), and triethyl phosphate (TEP, 98%) were bought from Aladdin. Poly(vinylidene fluoride) (PVDF) was provided by Alfa Aesar. Polyester non-woven fabric was supplied by Shanghai Tianluo Advanced Textile Co., Ltd. N-methyl pyrrolidone (NMP, ≥ 99.5%), methanol (≥ 99.5%), ethanol (≥ 99.5%), isopropanol (≥ 99.5%), *n*-propanol (≥ 99.5%), *n*-butanol (≥ 99.5%), *n*-hexane (≥ 99%), N,N-dimethylformamide (DMF, ≥ 99.9%), chloroform (CHCl$_3$, ≥ 99%), chloroform-*d* (≥ 99%), xylene (99%), and tetrahydrofuran (THF, ≥ 99.5%) were provided by Sinopharm Chemical Reagent Co., Ltd. All chemicals and reagents were used without further purification.

S2. Synthesis of APDMS-HDI/DDP elastomers

As illustrated in Fig. S1, a series of APDMS-HDI/DDP elastomers were synthesized by the polycondensation reaction between the APDMS macromer and the two diisocyanatos (HDI and DDP). The synthesized APDMS-HDI/DDP elastomers were designated as APDMS-HDI/DDP(x:y), where x:y stands for HDI/DDP mole ratio. The synthesis procedure of APDMS-HDI/DDP(5:5) was provided as an example as follows: APDMS (1 mmol, 2.5 g) and 5 mL THF were transferred into a 100 mL round-bottom flask equipped with a reflux condenser and a nitrogen inlet, which was later placed into ice bath for subsequent reaction. HDI (0.5 mmol, 0.084 g), DDP (0.5 mmol, 0.132 g), and 10 mL THF were added into a glass bottle, and then stirred to obtain a homogenous mixture. Afterwards, the mixture was added drop-by-drop to the above APDMS solution, to allow a 2-h reaction in an ice bath and followed by another 22-h reaction at 60 °C. Finally, the viscous elastomer solution was obtained and stored for the subsequent preparation of the supramolecular membrane. Component content for the synthesis of APDMS-HDI/DDP(x:y) elastomers was given in Table S1.
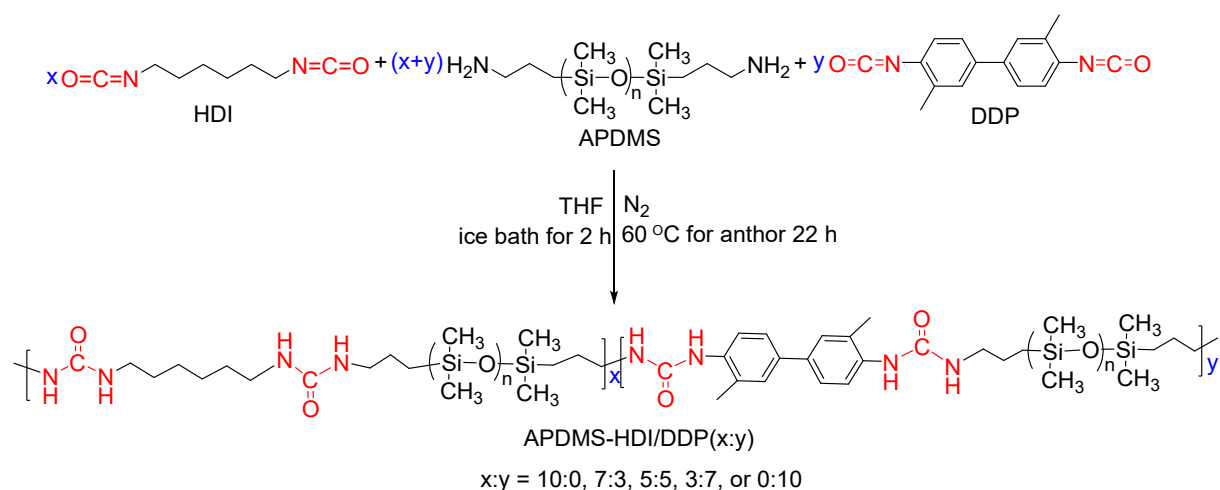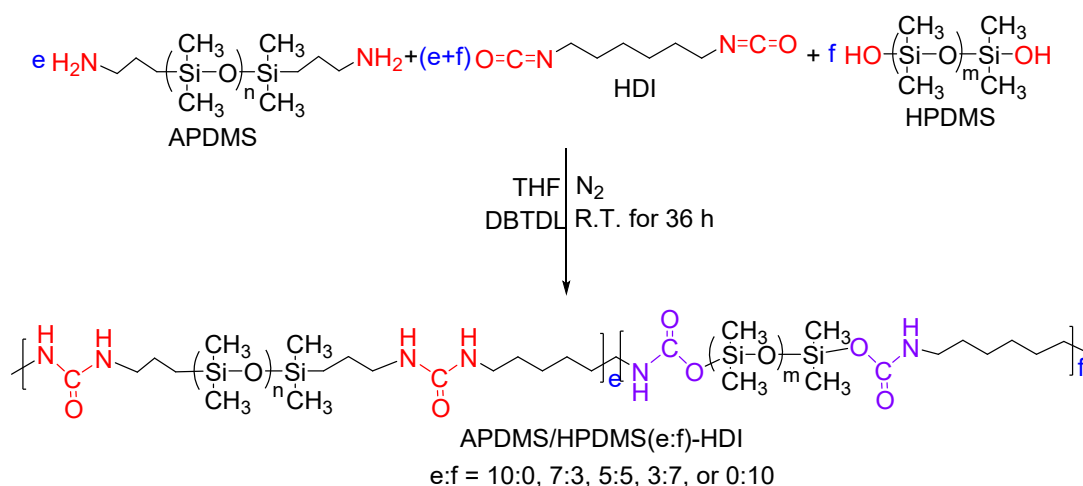

Fig. S1. Synthesis route of APDMS-HDI/DDP(x:y) elastomers (x:y = 10:0, 7:3, 5:5, 3:7, or 0:10).

Table S1. Component content for the synthesis of APDMS-HDI/DDP(*x:y*) elastomers (*x:y* = 10:0, 7:3, 5:5, 3:7, or 0:10).

Supramolecular elastomers	APDMS (mmol)	HDI (mmol)	DDP (mmol)
APDMS-HDI/DDP(10:0)	1	1	0
APDMS-HDI/DDP(7:3)	1	0.7	0.3
APDMS-HDI/DDP(5:5)	1	0.5	0.5
APDMS-HDI/DDP(3:7)	1	0.3	0.7
APDMS-HDI/DDP(0:10)	1	0	1

S3. Synthesis of APDMS/HPDMS-HDI elastomer

As shown in Fig. S2, a series of APDMS/HPDMS-HDI elastomers were synthesized by the polycondensation reaction between the PDMS macromers (APDMS and HPDMS) and HDI. The synthesized APDMS/HPDMS-HDI elastomers were abbreviated as APDMS/HPDMS(*e*:*f*)-HDI, where *e*:*f* refers to APDMS/HPDMS mole ratio. The synthesis procedure of APDMS/HPDMS(5:5)-HDI was provided as an example as follows: APDMS (0.5 mmol, 1.25 g), HPDMS (0.5 mmol, 1.38 g), and 5 mL THF were transferred into a 100 mL round-bottom flask equipped with a reflux condenser and a nitrogen inlet. HDI (1 mmol, 0.084 g), DBTDL (0.02 g), and 10 mL THF were added into a glass bottle, and then stirred to obtain a homogenous mixture. Afterwards, the mixture was added drop-by-drop to the above APDMS and HPDMS mixed solution, followed by a reaction at room temperature for 36 h. Finally, the viscous elastomer solution was obtained and stored for the subsequent preparation of the supramolecular membrane. Component content for the synthesis of APDMS/HPDMS(*e*:*f*)-HDI elastomers was given in Table S2.

Fig. S2. Synthesis route of APDMS/HPDMS(*e*:*f*)-HDI elastomers (*e*:*f* = 10:0, 7:3, 5:5, 3:7, or 0:10).

Table S2. Component content for the synthesis of APDMS/HPDMS(*e:f*)-HDI elastomers (*e:f* = 10:0, 7:3, 5:5, 3:7, or 0:10).

Supramolecular elastomers	APDMS (mmol)	HPDMS (mmol)	HDI (mmol)
APDMS/HPDMS(10:0)-HDI	1	0	1
APDMS/HPDMS(7:3)-HDI	0.7	0.3	1
APDMS/HPDMS(5:5)-HDI	0.5	0.5	1
APDMS/HPDMS(3:7)-HDI	0.3	0.7	1
APDMS/HPDMS(0:10)-HDI	0	1	1

S4. Preparation of PVDF substrate

The dope solution containing 18 wt% PVDF, 30 wt% TEP, 6 wt% PVP, and 46 wt% NMP was prepared at 80 °C under stirring for 24 h, and cast onto a polyester nonwoven fabric by a casting thickness of 150 μm at room temperature. The nascent PVDF membrane was immersed into a water coagulation bath immediately at room temperature for 48 h to remove the trapped TEP, PVP, and NMP. Finally, the PVDF substrate was freeze-dried for later use.

S5. Preparation of the supramolecular membranes

The viscous elastomer solution obtained as described in Sections S2 and S3 was diluted to a viscosity of ~120 mPa·s, and cast onto the PVDF substrate by a casting thickness of 100 μm. The nascent PDMS-based supramolecular membranes were then obtained after overnight dry at 40 ℃. These membranes were designated as APDMS-HDI/DDP(*x*:*y*) and APDMS/HPDMS(*e*:*f*)-HDI membranes, where *x*:*y* and *e*:*f* refer to HDI/DDP and APDMS/HPDMS mole ratios respectively. Besides, free-standing supramolecular membranes were also prepared for characterization purpose by pouring the casting solution with viscosity of ~120 mPa·s into a glass dish.

S6. Material and membrane characterizations

ATR-FTIR. The chemical structures of the supramolecular elastomers were confirmed by an attenuated total reflectance Fourier transform infrared spectroscopy (ATR-FTIR, Bruker VERTEX-70) within the wavenumber of 4000 - 500 cm^{-1}. All spectra were gained with 16 scans per at room temperature. Curve fitting of FTIR spectra of the supramolecular membranes was obtained by peakfit 4.0 software.

In-situ FTIR. The thermal response of H-bond in APDMS/HPDMS(3:7)-HDI membrane with the temperature increase (tested for every 10 °C rise from 30 °C to 100 °C) was characterized by in situ FTIR (Nicolet iS50R) within the wavenumber range of 4000 - 400 cm^{-1}.

^{1}HNMR. In order to investigate the conversion degree of the monomers, ^{1}HNMR spectra of HDI, DDP, APDMS, and APDMS-HDI/DDP(5:5) were recorded in chloroform-*d* using a nuclear magnetic resonance (NMR, Bruker AV4000, 400 MHz) at 30 °C.

LF-NMR. The attenuation curves and crosslinking densities of APDMS-HDI/DDP(5:5) and APDMS/HPDMS(5:5)-HDI membranes were characterized by low-field nuclear magnetic resonance (LF-NMR, MesoMR23-060H-I) at 30 °C.

GPC. The molecular weights and polydispersity index of the supramolecular elastomers were measured by a gel permeation chromatography (GPC, Agilent PL-GPC 50) with two PLgel columns (MIXED-B and MIXED-C). The GPC measurements were performed at 30 °C in THF with a flow rate of 1.0 mL/min using a refractive index detector.

DSC. The glass transition temperature (T_g) of the supramolecular elastomers was characterized by differential scanning calorimetric analysis (DSC, Netzsch STA 449C). The DSC measurements were carried out with a heating rate of 10 °C/min and temperature ranging from -150 °C to 150 °C under nitrogen atmosphere. All samples were dried overnight under vacuum at 60 °C prior to the DSC test.

XRD. X-ray diffraction (XRD, Siemens D5000) of APDMS-HDI/DDP-10:0, APDMS-HDI/DDP-5:5, and APDMS-HDI/DDP-0:10 membranes was performed in the range of approximately 5 - 60° (2θ) with the copper Kα (0.154 nm) as the source. The average d-spacing (d_{sp}) for the amorphous peak maxima was calculated using Bragg's equation [1, 2].

SEM. The cross-sectional morphologies of the supramolecular membranes were observed by scanning electron microscope (SEM, Nova NanoSEM 450). The cross-section was obtained by freeze-fracturing in liquid nitrogen. Prior to SEM observation, all samples were sputtered with gold for 120 s.

Rheological properties. Dynamic rheological properties of free-standing supramolecular membranes were assessed by a modular compact rheometer (Anton paar, MCR 302). The free-standing membrane with ~ 2 mm thicknesses were cut into the circular samples with a diameter of 25 mm, and then transferred to an aluminum parallel plate with a diameter of 25 mm. It is noteworthy that APDMS/HPDMS(0:10)-HDI sample with poor membrane formation ability was cast directly on the surface of aluminum parallel plate. All samples were tested at the frequency of 1 Hz and 25 °C. The storage modulus (G′), loss modulus (G″), phase angle (δ) and loss factor (tanδ, G″/G′) were recorded from strain response. All measurements were carried out within linear viscoelastic region.

DMTA. Dynamic mechanical thermal analysis (DMTA, PerkinElmer Instruments, DMS6100) was employed to characterize the dynamic mechanical properties of free-standing supramolecular membranes. Each sample with dimensions of ~0.6 mm (length) × 10 mm (width) × 10 mm (thickness) was tested at the frequency of 1 Hz and the temperature range of -150 °C to 0 °C under compression mode.

Contact angle. Water and ethanol contact angles of the supramolecular membranes were measured with a contact angle goniometer (KRÜSS DSA 25) using the sessile drop method in air. The dried membrane was locked to the glass sheet, and a drop of 5 μL droplet was dropped on the surface of the membrane to measure the contact angle. At least 3 points were obtained for each membrane to get an average value.

Solution viscosity. Casting solution viscosity was measured by a digital viscometer (NDJ-5S) with a speed of 60 rpm at 25 °C.

Solubility property. Covalently-crosslinked PDMS-TEOS elastomer was prepared according to our previous work [3]. 10 g PDMS, 1 g TEOS, and 0.1 DBTDL were added into 50 mL *n*-hexene, and stirred for 10 min. After that, the mixture was poured into a glass dish, followed by curing at 30 °C overnight and then at 60 °C for another 6 h for further curing. In order to evaluate the solubility properties of H-bond crosslinked supramolecular and covalently-crosslinked PDMS-TEOS elastomers, APDMS-HDI/DDP(5:5) and PDMS-TEOS elastomers were immersed into THF, *n*-hexene, CHCl$_3$, xylene, DMF, and NMP solvents respectively,

and then placed at 30 °C for 24 h. Considering the good transmittance of both the elastomer samples and the solvents used, the solubility properties were judged by close observing the presence of undissolved sample in the drained solvents after the immersion of samples.

Solvent uptake. The sample strips of free-standing supramolecular membranes were dried under vacuum at 60 °C for 6 h, and then immersed into feed solution (5 wt% ethanol aqueous solution) at room temperature (~ 22 °C) for 4 days. After these strips were taken out from the immersion solution, the liquid adhering on the surface of the strips was wiped off with a tissue paper. The solvent uptake (%) was calculated by *eq.* (S1) [4],

$$Solvent\ uptake\ (\%) = \frac{W_{wet} - W_{dry}}{W_{dry}} \times 100\%$$

(S1)

where W_{dry} and W_{wet} refer to the weights of the membrane strips before and after sorption.

Pervaporation test. Pervaporation test was performed using a lab-scale cell with an effective membrane area of 11.33 cm^2. The schematic diagram of the pervaporation separation test was reported in our previous works [3, 5]. 5 wt% alcohol aqueous solution (methanol, ethanol, isopropanol, or n-butanol) as feed solution was contacted with the top surface of the membranes, while the permeate side was maintained vacuum (less than 3 mbar). Prior to the sample collection, the test system was pre-conditioned over 2 h to reach the mass transfer equilibrium. For each sample, at least three permeates were collected from the cold trap immersed in liquid nitrogen. The alcohol concentrations in feed and permeate were detected by an Agilent 7890A gas chromatograph. The pervaporation performance was assessed by

total flux (J, g/m^2 h) and separation factor (α) as follow [6-8]:

$$J = \frac{w}{A \times t}$$

(S2)

$$\alpha = \frac{y_p/(1 - y_p)}{x_f/(1 - x_f)}$$

(S3)

where w, A, and t refer to the weight of the permeate (g), the effective membrane area (cm^2), and the permeation time (h), respectively. x_f and y_p are the weight fractions of alcohol in feed and permeate, respectively.

In order to eliminate the effect of the thickness of the selective layer on the total flux, normalized total flux (J', μm·kg/m^2 h) was also used to assess the membrane separation performance according to the following *eqn* (S4) [9],

$$J' = J \times l$$

(S4)

where l is the thickness of the selective layer, as illustrated in Figs. S14, S16, and S17.

In order to exclude the effect of driving force, the intrinsic separation properties of pervaporation membrane, i.e., permeability (P_i, Barrer, 1 Barrer = 10^{-10} cm^3 (STP) cm/cm^2·s·cmHg) and selectivity (β), were further determined by *eqns.* (S5) and (S6) [10-12],

$$P_i = \frac{J_i \times l}{\gamma_{i,f}\chi_{i,f}P_{i,f}^{sat} - P_{i,p}}$$

(S5)

$$\beta = \frac{P_E}{P_W}$$

(S6)

where J_i (mol/m^2 h) is the mole flux of the component i in permeate, $P_{i,p}$ (kPa) is the individual permeate pressure of the component i, which is generally negligible, $\gamma_{i,f}$ calculated by software Aspen 8.0 refers to the activity coefficient of the component i in the feed side, $\chi_{i,f}$

stands for the mole fraction of the component i in feed, $Psat_{i,f}$ (kPa) refers to the saturation vapor pressure of the component i in the feed side, P_E and P_W are the permeabilities of ethanol and water, respectively.
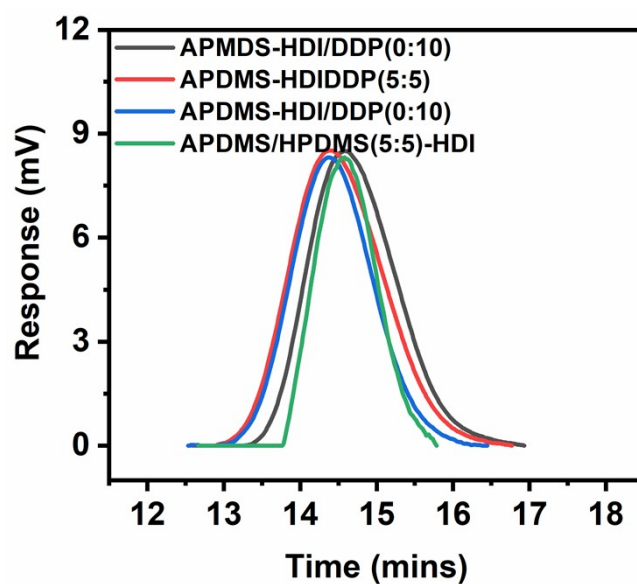
S7. FTIR results of PDMS-based supramolecular membranes
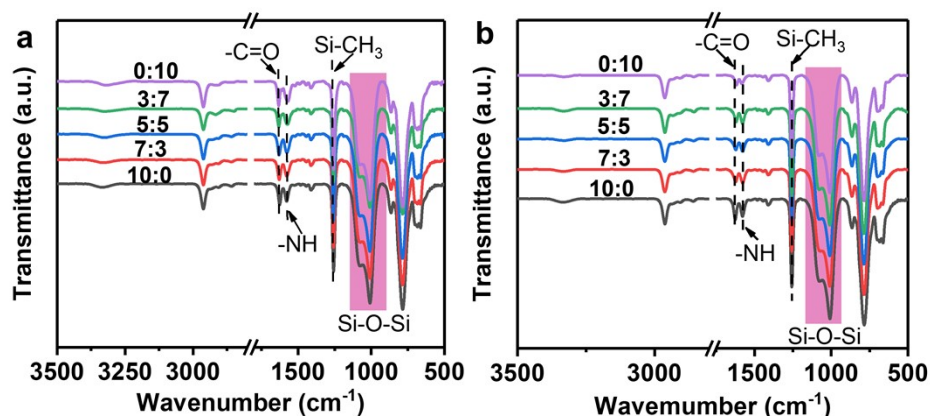
Fig. S3. FTIR spectra of (a) APDMS-HDI/DDP(x:y) and (b) APDMS/HPDMS(e:f)-HDI membranes. (The number on the curves refer to the mole ratios HDI/DDP(x:y) and APDMS/HPDMS(e:f) respectively).
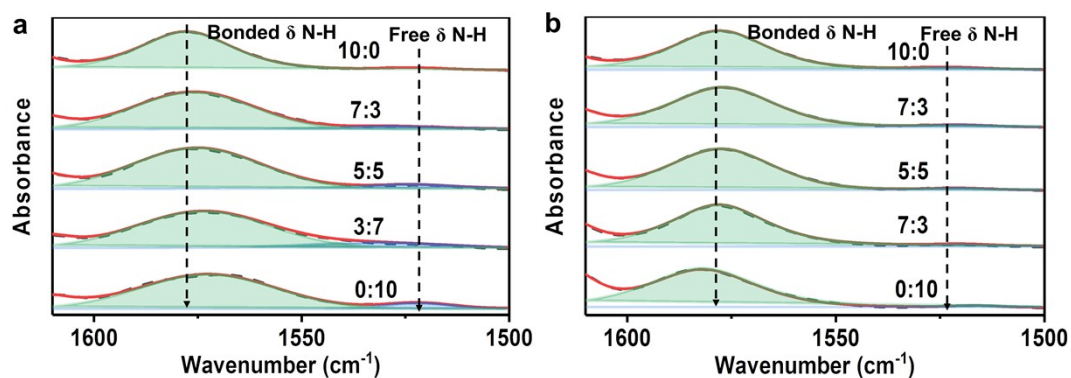
Fig. S4. Curve fitting of FTIR spectra of (a) APDMS-HDI/DD(x:y) and (b) APDMS/HPDMS(e:f)-HDI membranes.

S8. GPC results

Fig. S5. GPC curves of APDMS-HDI/DDP(0:10), APDMS-HDI/DDP(5:5), APDMS-HDI/DDP(10:0), and APDMS/HPDMS(5:5)-HDI elastomers.

Table S3. Molecular weights and polydispersity index of APDMS-HDI/DDP(0:10), APDMS-HDI/DDP(5;5), APDMS-HDI/DDP(10:0), and APDMS/HPDMS(5:5)-HDI elastomers.

| Supramolecular elastomers	Molecular weights (M_n, kDa)	Polydispersity index
APDMS-HDI/DDP(0:10)	24	1.5
APDMS-HDI/DDP(5;5)	30	1.6
APDMS-HDI/DDP(10:0)	35	1.4
APDMS/HPDMS(5:5)-HDI	31	1.2

S9 In-situ FTIR result of APDMS/HPDMS(3:7)-HDI membrane
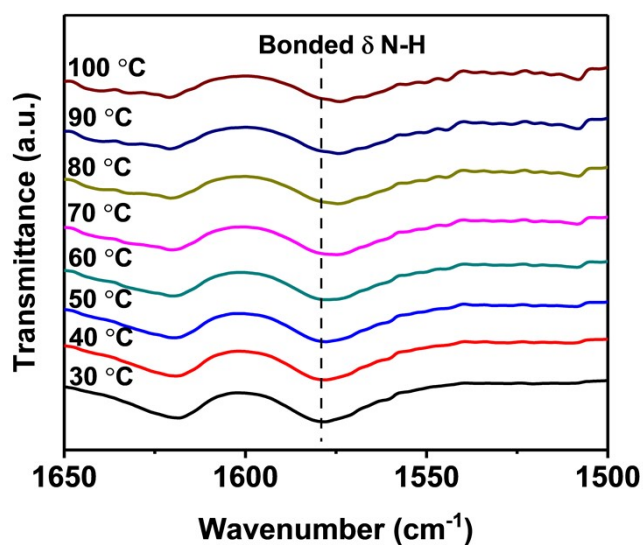
Fig. S6. In-situ FTIR spectra of APDMS/HPDMS(3:7)-HDI membrane in the temperature range of 30 - 100 ℃.

The thermal response of H-bond in APDMS/HPDMS(3:7)-HDI membrane with the temperature increase was characterized by in-situ FTIR (Fig. S6). It can be found that, the characteristic peak of bonded δ N-H group (~1580 cm^{-1}) is blue-shifted with the temperature increase, signifying the weaker H-bond [13]. This result also verifies the presence of H-bond in the PDMS-based supramolecular membranes.
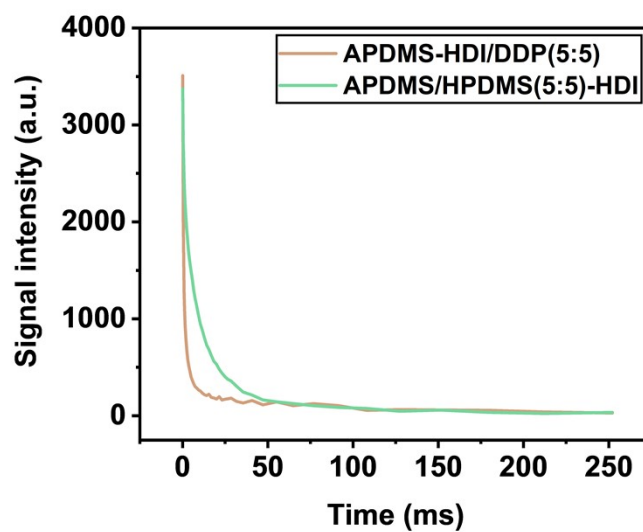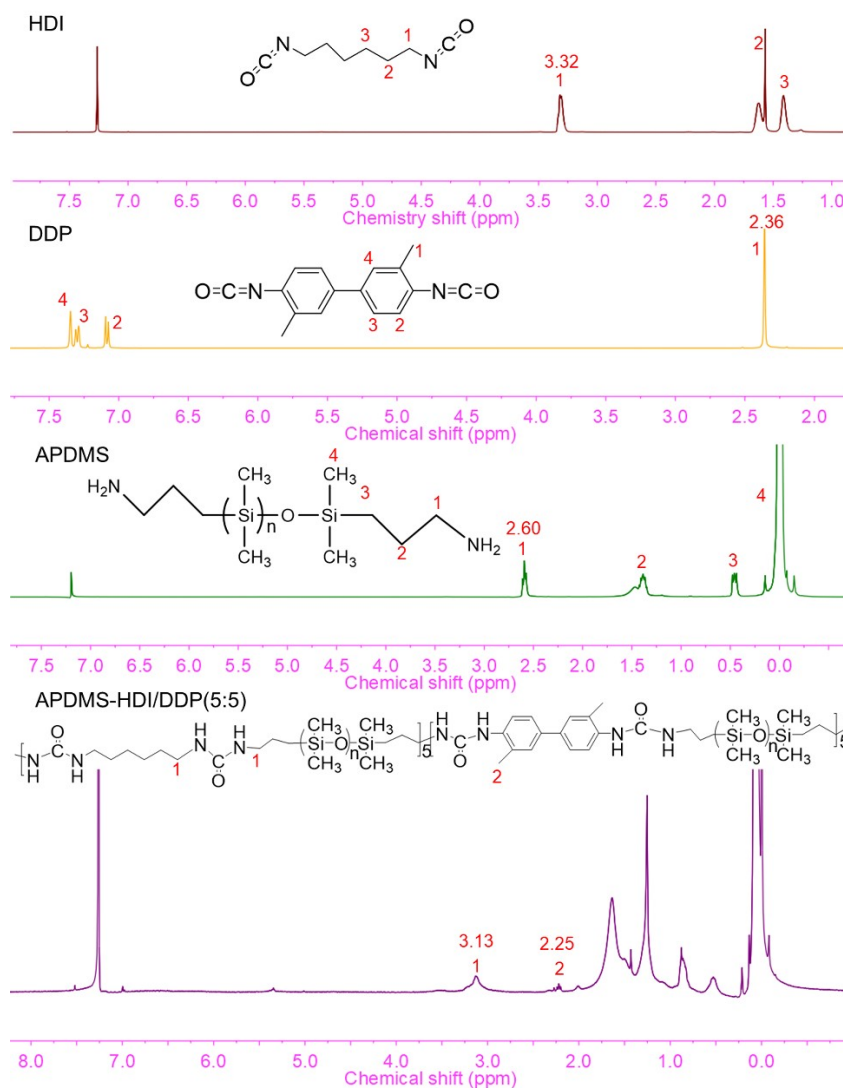
Fig. S7. Attenuation curves of APDMS-HDI/DDP(5:5) and APDMS/HPDMS(5:5)-HDI membranes.

Table S4. Crosslinking densities of APDMS-HDI/DDP(5:5) and APDMS/HPDMS(5:5)-HDI membranes.

| Membrane	Crosslinking density (10^{-4} mol/mL)
APDMS-HDI/DDP(5:5)	7.74
APDMS/HPDMS(5:5)-HDI	2.65

Fig. S8. ¹HNMR spectra of HDI, DDP, APDMS, and APDMS-HDI/DDP(5:5).

¹HNMR spectra of HDI, DDP, APDMS, and APDMS-HDI/DDP(5:5) are recorded to investigate the conversion degree of the monomers. As illustrated in Fig. S8, the characteristic peaks 1 (3.13 ppm) and 2 (2.25 ppm) appear in the ¹HNMR spectrum of APDMS-HDI/DDP(5:5), verifying the successful reaction among HDI, DDP, and APDMS. Furthermore, no characteristic peaks of unreacted monomers (HDI (3.32 ppm), DDP (2.36 ppm), and APDMS (2.60 ppm)) are observed in the ¹HNMR spectrum of APDMS-HDI/DDP(5:5), suggesting the full reaction degree of the monomers.
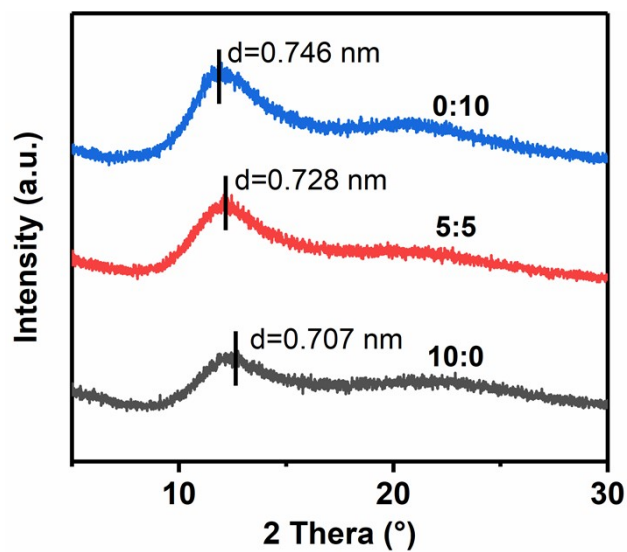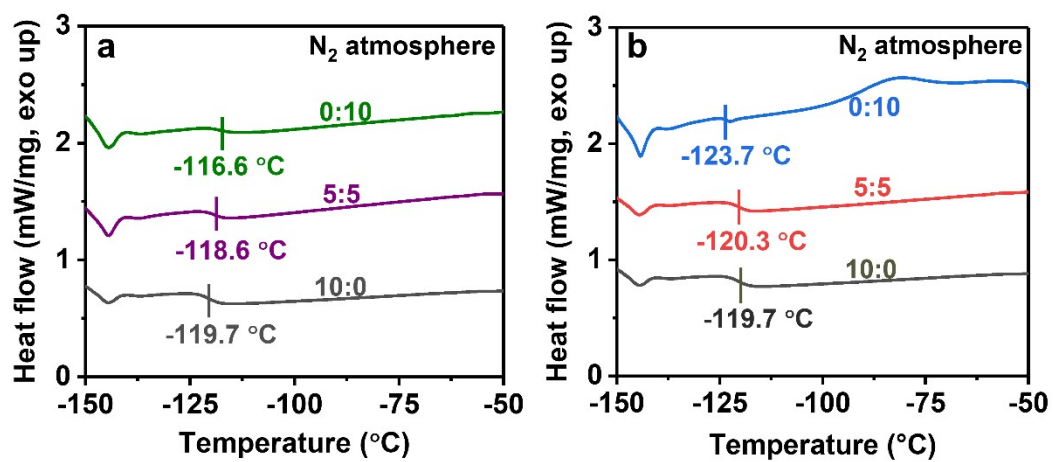
Fig. S9. XRD patterns of APDMS-HDI/DDP(*x:y*) membranes (*x:y* = 10:0, 5:5, and 0:10).

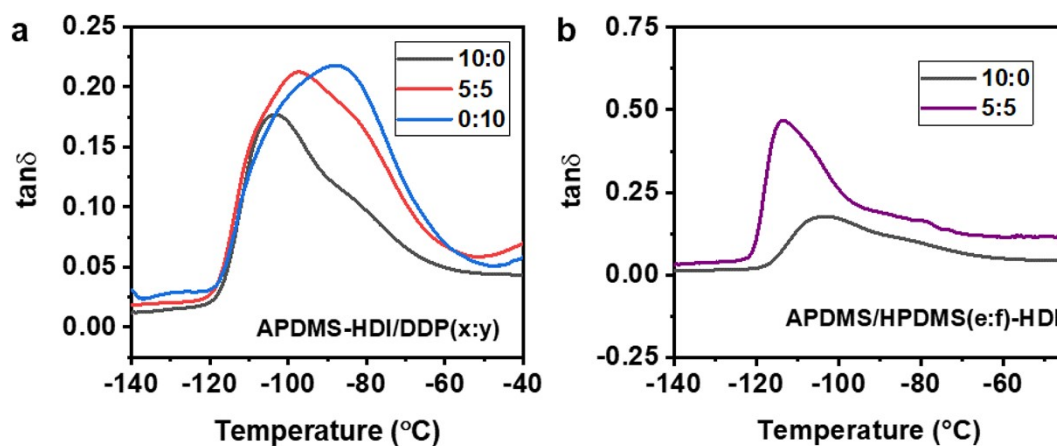With the increase in rigid DDP content, the *d*-spacing gradually increases, indicative of the
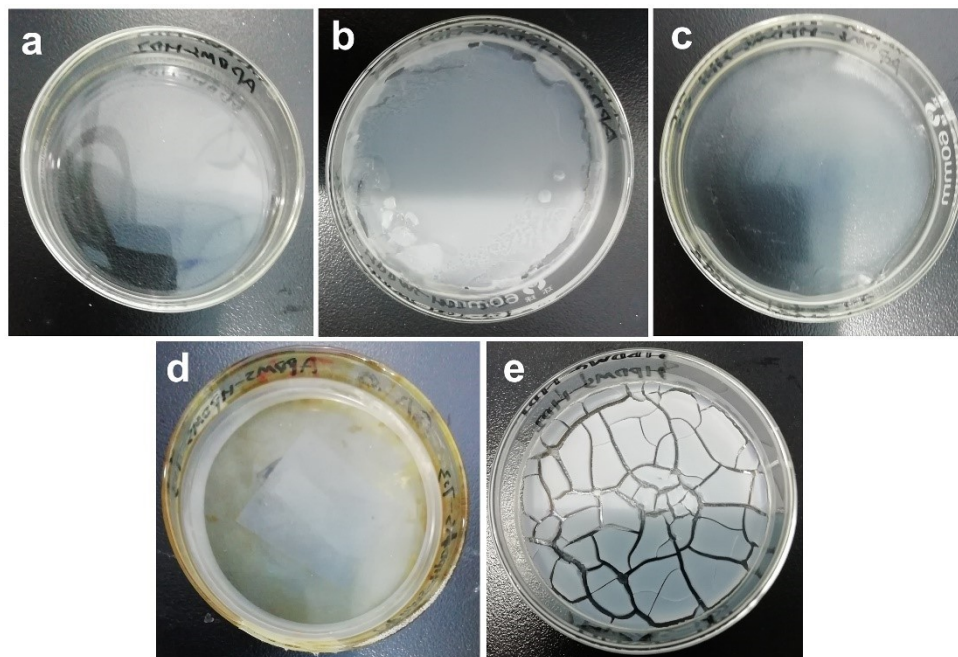
larger chain distance.

Fig. S10. DSC curves of (a) APDMS-HDI/DDP(*x:y*) and (b) APDMS/HPDMS(*e:f*)-HDI

membranes. (Note: x:y and e:f =10:0, 5:5, or 0:10)

Fig. S11. DMTA cures of (a) APDMS-HDI/DDP(*x:y*) and (b) APDMS/HPDMS(*e:f*)-HDI membranes.(*x:y* = 10:0, 5:5, and 0:10; *e:f* = 10:0 and 5:5)

Fig. S12. Digital photos of free-standing (a) APDMS/HPDMS(10:0)-HDI, (b) APDMS/HPDMS(3:7)-HDI, (c) APDMS/HPDMS(5:5)-HDI, (d) APDMS/HPDMS(7:3)-HDI, and (e) APDMS/HPDMS(0:10)-HDI membranes.

As shown in Fig. S12, all free-standing membranes have good membrane formation ability, except the free-standing APDMS/HPDMS(0:10)-HDI membrane with a very low H-bond content (3.43×10^{-4} mol/g).
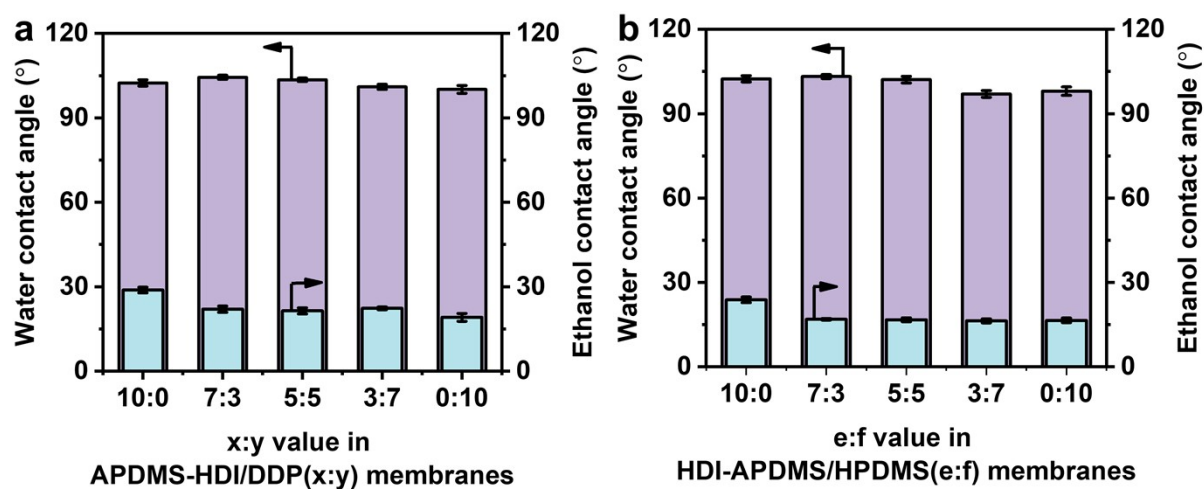
Fig. S13. Surface water and ethanol contact angles of (a) APDMS-HDI/DDP(*x:y*) and (b) APDMS/HPDMS(*e:f*)-HDI membranes.

The surface water contact angles of PDMS-based supramolecular membranes are significantly higher than their ethanol contact angles, indicating the stronger affinity of PDMS-based supramolecular membranes toward ethanol molecules [14]. Furthermore, it can be found from Fig. S13 that, both water and ethanol contact angles of the PDMS-based supramolecular membranes decrease insignificantly with the increase in HDI/DDP and APDMS/HPDMS mole ratios, probably attributed to the reduction of hydrophobic alkyl structural ratios in the membranes.

1200 mpa·s

23.1±0.5 μm

600 mpa·s

13.5±0.3 μm

360 mpa·s

10.9±0.1 μm

20 μm

120 mpa·s

5.1±0.2 μm

80 mpa·s

2.5±0.1 μm
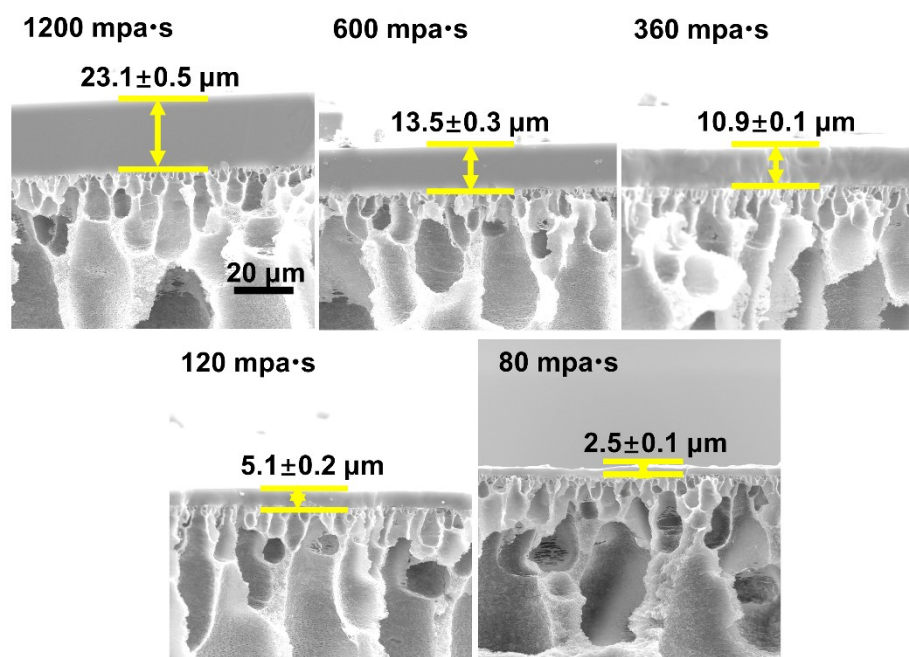
Fig. S14. The cross-sectional morphologies and thicknesses of APDMS-HDI/DDP(5:5) membranes prepared by casting solutions of different viscosities.

Fig. S15. Pervaporation performance of APDMS-HDI/DDP(5:5) membranes prepared by casting solutions of different viscosities in separating 5 wt% ethanol aqueous solution at 60 °C.

Basically, the thinner the selective layer of the membrane, the greater the permeation flux, provided that the selective layer is defect-free. Thereupon, the thickness of the selective layer of APDMS-HDI/DDP(5:5) membrane (as an example) is tuned by controlling the viscosities of the casting solutions from 1200 to 80 mpa·s. The result in Fig. S14 shows that, the thickness of the selective layer gradually decreases from 23.1 to 2.5 μm, and the corresponding ethanol/water separation performance changes as illustrated in Fig. S15. As expected, the total flux increases, attributed to the reduction of mass transport resistance, while the ethanol/water separation factor remains constant initially and then reduces sharply due to the possible defects caused by the overthin selective layer. Consequently, a series of the supramolecular membranes are fabricated by the optimal casting solutions with the viscosity of ~120 mpa·s.
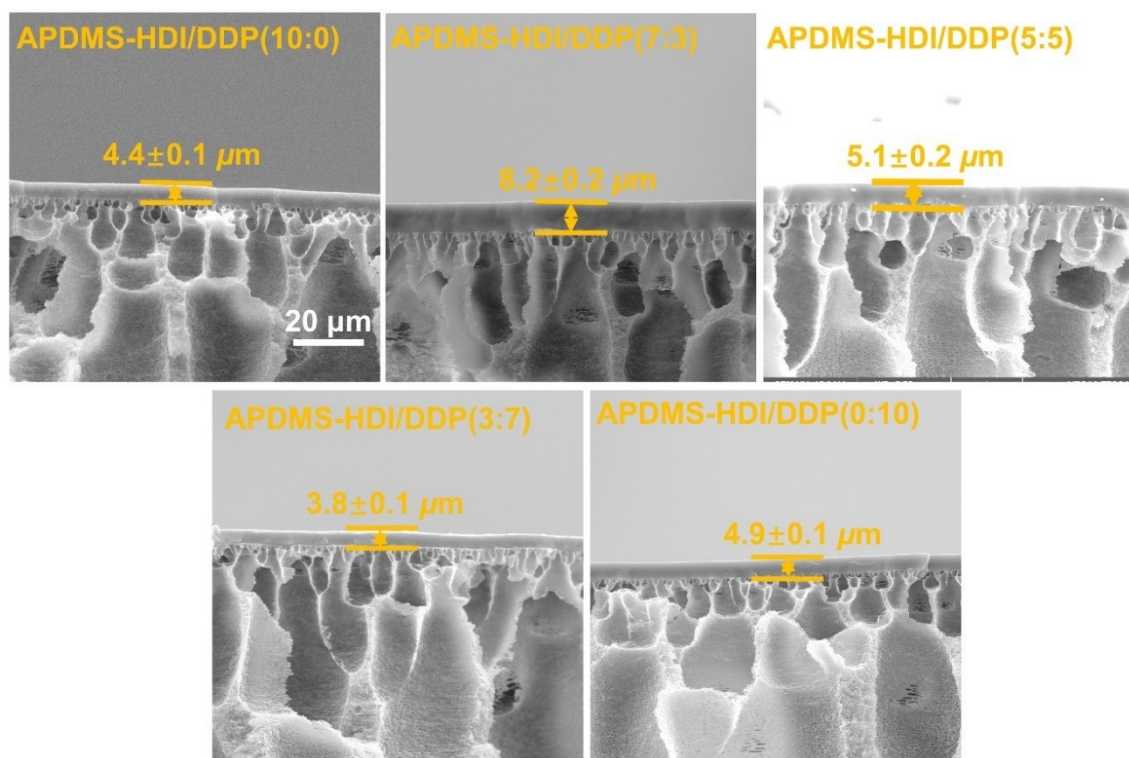
Fig. S16. The cross-sectional morphologies and thicknesses of APDMS-HDI/DDP(*x:y*) membranes (*x:y* = 10:0, 7:3, 5:5, 3:7, or 0:10).
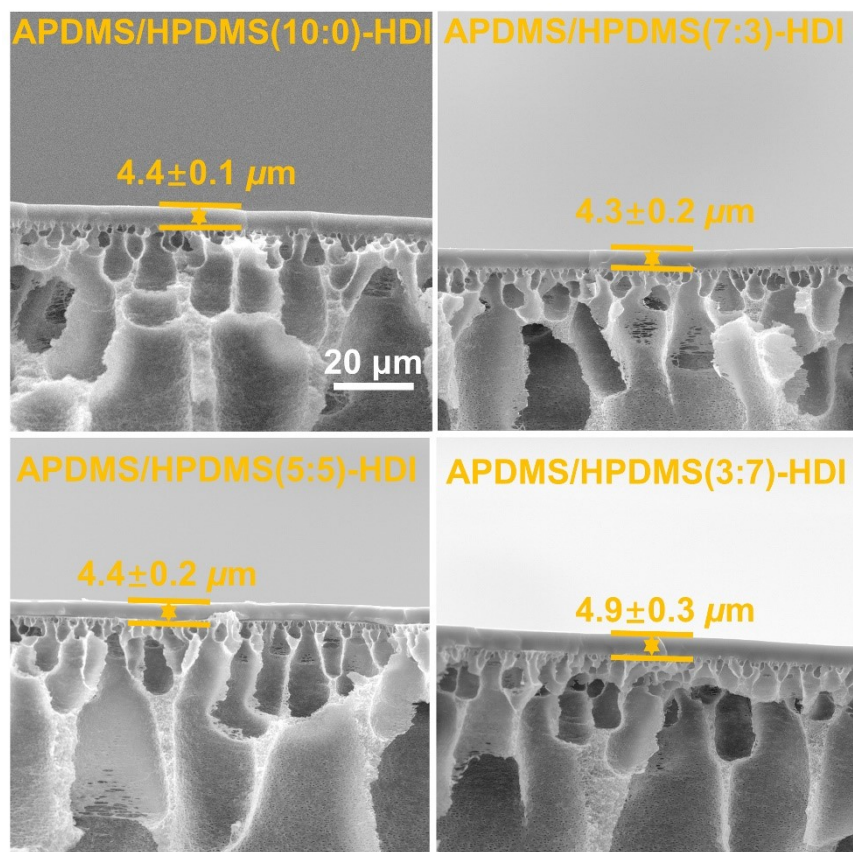
Fig. S17. The cross-sectional morphologies and thicknesses of APDMS/HPDMS(*e:f*)-HDI membranes (*e:f* = 10:0, 7:3, 5:5, or 3:7).

S20. Hildebrand solubility parameter of APDMS/HPDMS(3:7)-HDI elastomer

The Hildebrand solubility parameter (δ_{sp}, MPa$^{1/2}$) is defined as the square root of the cohesive

energy density [15-17],

$$\delta_{sp} = (\frac{E}{V})^{0.5} = \left(\frac{\sum E_{coh}}{\sum V_i}\right)^{0.5}$$

(S7)

where E is the total cohesive energy of the elastomer (cal/mol), V is the total mole volume of

the elastomer (cm^3/mol); E_{coh} refers to the cohesive energy of each structural unit in the

elastomer (cal/mol), Vi is the mole volume of each structural unit in the elastomer (cm^3/mol).

The numerical value of the solubility parameter in MPa$^{1/2}$ is 2.0455 times larger than that in

(cal/cm^3)$^{1/2}$.
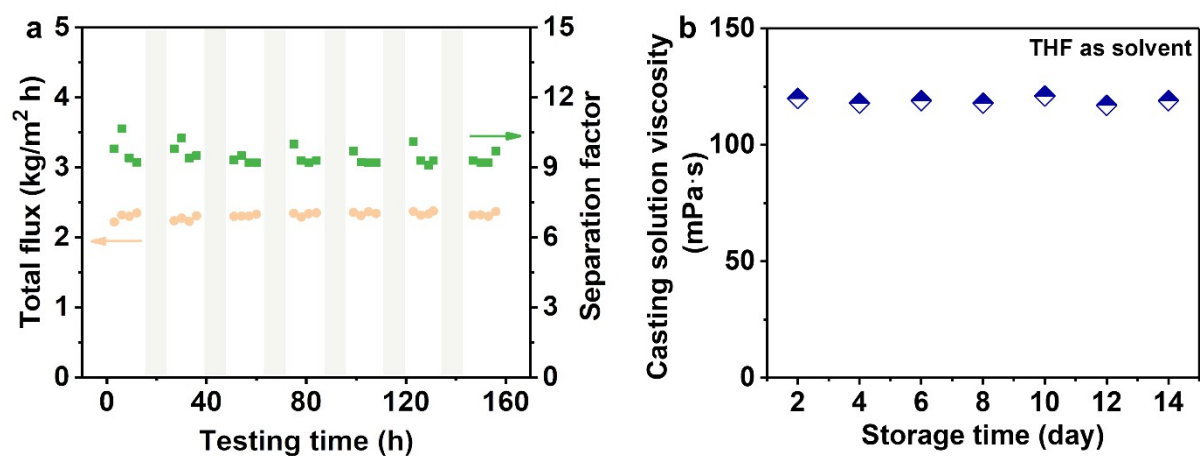
Fig. S18. (a) Long-term stability of APDMS/HPDMS(3:7)-HDI membrane with 5 wt% ethanol aqueous solution at 60 °C (no vacuum during night, marked by light-blue areas). (b) Long-term stability of APDMS/HPDMS(3:7)-HDI casting solution.
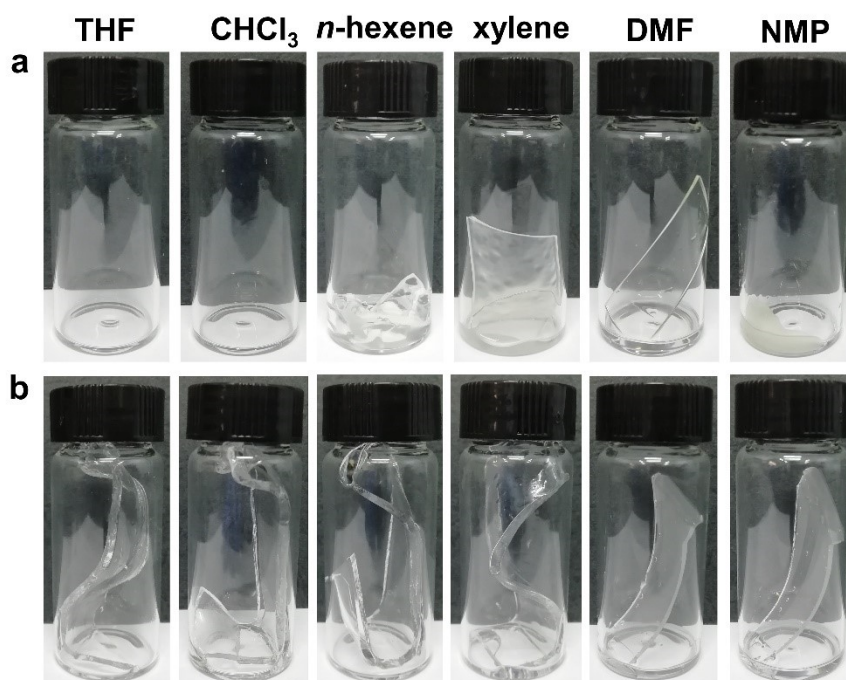
Fig. S19. Digital pictures of (a) APDMS-HDI/DDP(5:5) and (b) covalently-crosslinked PDMS elastomers after 24-h immersion in the solvent (solvent was poured out for better observation).

Table S5. Solubility properties of APDMS-HDI/DDP(5:5) and covalently-crosslinked PDMS elastomers.

elastomers	THF	CHCl$_3$	*n*-hexene	xylene	DMF	NMP
APDMS-HDI/DDP(5:5)	++	++	+	--	--	+
covalently-crosslinked PDMS	--	--	--	--	--	--

++: soluble, +: partially soluble, --: insoluble.

S23. Performance benchmarking

Table S6. Performance comparison with other reported polymeric membranes for ethanol recovery from aqueous solution.

Membrane	Ethanol concentration in feed (wt%)	Operation Temperature (°C)	Total flux (kg/m² h)	Separation factor	Ref.
PDMS	5	40	1.3	8.5	[18]
	5	50	~0.75	5.8	[19]
	5	40	0.49	5.4	[20]
	5	60	0.866	6.8	[21]
	5	70	1.667	7.6	[22]
	5	60	0.828	8.5	[23]
	5	50	0.149	9.2	[24]
	5	60	1.186	8.2	[25]
	5	60	0.225	7.5	[26]
	5	60	0.86	9.2	[27]
	5	6	1.418	8.2	[28]
	5	40	2.4	8.6	[29]
	5	40	0.435	6.4	[4]
	5	40	0.381	5.7	[3]
	5	40	~1.35	~7.5	[13]
	5	24	2.4	7.2	[30]
	5	40	1.6	8.9	[31]
Pebax	5	40	~0.63	~3.0	[32]
	5	23	0.117	2.5	[33]
	5	25	0.08	~2.5	[34]
PIM-1	5	60	0.691	3.61	[35]
	5	65	9.08	13.3	[36]
	5	65	~0.833	3.1	[37]
APDMS/HPD MS(3:7)-HDI	5	40	1.11	8.3	This work
		50	1.60	8.5	
		60	2.27	9.7	
		70	3.16	8.9	
		80	4.12	8.5	

Note: ~ refers to the data estimated from the performance graph in the literature.

Table S7. Performance comparison with other reported polymeric membranes for *n*-butanol recovery from aqueous solution.

Membrane	*n*-butanol concentration in feed (wt%)	Operation Temperature (°C)	Total flux (kg/m² h)	Separation factor	Ref
PDMS	1	50	0.312	36.4	38
	1	40	0.282	38.6	39
	1.5	55	1.538	47	40
	1.5	55	1.100	45	41
	3.6	34	0.803	24.2	42
	1.5	55	0.779	~42.5	43
	5	40	1.011	51	44
	1	40	0.822	34.5	45
	1.5	55	1.075	41	46
	1.5	55	0.590	45	47
	1.5	55	1.340	39.7	48
	1	42	1.390	22	49
	1	70	2.210	46	50
	1	60	~1.200	12	51
	1	60	0.843	51.7	52
	1	60	1.080	51	53
Pebax	2	40	~0.88	~15.5	54
PIM-1	5	20	~0.54	~6.5	55
	5	65	~1.132	13.5	37
	5	30	~0.92	~13	56
APDMS/HPDMS(3:7)-HDI	1	60	2.05	26.7	This work
	5	40	1.95	15.8	
		50	2.96	16.2	
		60	4.23	16.0	
		70	5.76	15.1	
		80	7.75	14.2	

Note: ~ refers to the data estimated from the performance graph in the literature.

References

1. T. Zhu, X. Yang, X. He, Y. Zheng and J. Luo, *High Perform. Polym.*, 2017, **30**, 821-832.

2. T. Zhu, X. Yang, Y. Zhang, Y. Zheng, X. He and J. Luo, *J. Nat. Gas Sci. Eng.*, 2018, **54**, 92-101.

3. T. Zhu, S. Xu, F. Yu, X. Yu and Y. Wang, *J. Membr. Sci.*, 2020, **598**, 117681.

4. T. Zhu, X. Yu, M. Yi and Y. Wang, *ACS Sustain. Chem. Eng.*, 2020, **8**, 12664-12676.

5. Y. Pan, T. Zhu, Q. Xia, X. Yu and Y. Wang, *J. Environ. Chem. Eng.*, 2021, **9**, 104977.

6. Y. K. Ong, G. M. Shi, N. L. Le, Y. P. Tang, J. Zuo, S. P. Nunes and T. S. Chung, *Prog. Polym. Sci.*, 2016, **57**, 1-31.

7. L. Y. Jiang, Y. Wang, T.-S. Chung, X. Y. Qiao and J.-Y. Lai, *Prog. Polym. Sci.*, 2009, **34**, 1135-1160.

8. T. Zhu, S. Liu, Q. Xia, M. Yi, H. Liu, H. Dong and Y. Wang, *Chem. Eng. J.*, 2022, **448** 137773.

9. S. Xu, H. Zhang, F. Yu, X. Zhao and Y. Wang, *Sep. Purif. Technol.*, 2018, **206**, 80-89.

10. A. E. Ozcam, N. Petzetakis, S. Silverman, A. K. Jha and N. P. Balsara, *Macromolecules*, 2013, **46**, 9652-9658.

11. L. H. Wee, Y. Li, K. Zhang, P. Davit, S. Bordiga, J. Jiang, I. F. J. Vankelecom and J. A. Martens, *Adv. Funct. Mater.*, 2015, **25**, 516-525.

12. S. Yi and Y. Wan, *Chem. Eng. J.*, 2017, **313**, 1639-1646.

13. H. Chen, J. J. Koh, M. Liu, P. Li, X. Fan, S. Liu, J. C. C. Yeo, Y. Tan, B. C. K. Tee and C. He, *ACS Appl. Mater. Interfaces*, 2020, **12**, 31975-31983.

14. H. Mao, H. G. Zhen, A. Ahmad, A. S. Zhang and Z. P. Zhao, *J. Membr. Sci.*, 2019, **573**, 344-358.

15. C. M. Hansen, *Second Edition (2nd ed.)*, *CRC Press*, 2007.

16. E. Stefanis and C. Panayiotou, *Int. J. Thermophys.*, 2008, **29**, 568-585.

17. C. Özdemir and A. Güner, *Eur. Polym. J.*, 2007, **43**, 3068-3093.

18. L. Li, Z. Xiao, S. Tan, L. Pu and Z. Zhang, *J. Membr. Sci.*, 2004, **243**, 177-187.

19. Y. Li, L. H. Wee, J. A. Martens and I. F. J. Vankelecom, *J. Mater. Chem. A*, 2014, **2**, 10034-10040.

20. Y. Pan, R. Xie, B. Xu and C. Chen, *Micropor. Mesopor. Mater.*, 2021, **320**, 111086.

21. N. Wang, G. Shi, J. Gao, J. Li, L. Wang, H. Guo, G. Zhang and S. Ji, *Sep. Purif. Technol.*, 2015, **153**, 146-155.

22. G. Zhang, J. Li, N. Wang, H. Fan, R. Zhang, G. Zhang and S. Ji, *J. Membr. Sci.*, 2015, **492**, 322-330.

23. J. Li, S. Ji, G. Zhang and H. Guo, *Langmuir*, 2013, **29**, 8093-8102.

24. X. Zhan, J. Lu, T. Tan and J. Li, *Appl. Surf. Sci.*, 2012, **259**, 547-556.

25. H. Yan, J. Li, H. Fan, S. Ji, G. Zhang and Z. Zhang, *J. Membr. Sci.*, 2015, **481**, 94-105.

26. X. Zhan, M. Wang, T. Gao, J. Lu, Y. He and J. Li, *Sep. Purif. Technol.*, 2020, **236**, 116238.

27. J. Liu, J. Chen, X. Zhan, M. Fang, T. Wang and J. Li, *Sep. Purif. Technol.*, 2015, **150**, 257-267.

28. C. Liu, T. Xue, Y. Yang, J. Ouyang, H. Chen, S. Yang, G. Li, D. Cai, Z. Si, S. Li and

P. Qin, *Chem. Eng. Res. Des.*, 2021, **168**, 13-24.

29.   C. Zong, X. Yang, D. Chen, Y. Chen, H. Zhou and W. Jin, *Sep. Purif. Technol.*, 2021, **255**, 117729.

30.   T. Puspasari, T. Chakrabarty, G. Genduso and K. V. Peinemann, *J. Mater. Chem. A*, 2018, **6**, 13685-13695.

31.   W. Wei, S. Xia, G. Liu, X. Dong, W. Jin and N. Xu, *J. Membr. Sci.*, 2011, **375**, 334-344.

32.   J. Gu, X. Shi, Y. Bai, H. Zhang, L. Zhang and H. Huang, *Chem. Eng. Technol.*, 2009, **32**, 155-160.

33.   F. Liu, L. Liu and X. Feng, *Sep. Purif. Technol.*, 2005, **42**, 273-282.

34.   N. L. Le, Y. Wang and T. S. Chung, *J. Membr. Sci.*, 2011, **379**, 174-183.

35.   C. R. Mason, M. G. Buonomenna, G. Golemme, P. M. Budd, F. Galiano, A. Figoli, K. Friess and V. Hynek, *Polymer*, 2013, **54**, 2222-2230.

36.   L. Gao, M. Alberto, P. Gorgojo, G. Szekely and P. M. Budd, *J. Membr. Sci.*, 2017, **529**, 207-214.

37.   M. Alberto, J. M. Luque-Alled, L. Gao, M. Iliut, E. Prestat, L. Newman, S. J. Haigh, A. Vijayaraghavan, P. M. Budd and P. Gorgojo, *J. Membr. Sci.*, 2017, **526**, 437-449.

38.   L. H. Xu, S. H. Li, H. Mao, A. S. Zhang, W. W. Cai, T. Wang and Z. P. Zhao, *J. Mater. Chem. A*, 2021, **9**, 11853-11862.

39.   H. Mao, S. H. Li, A. S. Zhang, L. H. Xu, J. J. Lu and Z. P. Zhao, *J. Membr. Sci.*, 2020, **595**, 117543.

40.   Z. Si, J. Li, L. Ma, D. Cai, S. Li, J. Baeyens, J. Degreve, J. Nie, T. Tan and P. Qin,

Angew. Chem. Int. Ed., 2019, **131**, 17335-17339.

41.   Z. Si, C. Liu, G. Li, Z. Wang, J. Li, T. Xue, S. Yang, D. Cai, S. Li, H. Zhao, P. Qin and T. Tan, *J. Membr. Sci.*, 2020, **612**, 118472.

42.   G. Wu, X. Lu, Y. Li, Z. Jia, X. Cao, B. Wang and P. Zhang, *Sep. Purif. Technol.*, 2020, **241**, 116406.

43.   G. Li, Z. Si, D. Cai, Z. Wang, P. Qin and T. Tan, *Sep. Purif. Technol.*, 2020, **236**, 116263.

44.   J. Y. Lee, J. S. Lee and J. H. Lee, *Sep. Purif. Technol.*, 2020, **235**, 116142.

45.   J. Y. Lee, H. Park, J. S. Lee, S. Yoon and J. H. Lee, *J. Membr. Sci.*, 2019, **598**, 117654.

46.   Z. Si, S. Hu, D. Cai, P. Qin and Q. Xu, *RSC Adv.*, 2018, **8**, 5127-5135.

47.   Z. Si, D. Cai, S. Li, G. Li, Z. Wang and P. Qin, *Sep. Purif. Technol.*, 2019, **221**, 286-293.

48.   S. Hu, W. Ren, D. Cai, T. C. Hughes, P. Qin and T. Tan, *J. Membr. Sci.*, 2017, **533**, 270-278.

49.   J. Niemistö, W. Kujawski and R. L. Keiski, *J. Membr. Sci.*, 2013, **434**, 55-64.

50.   Y. Pan, Y. Hang, X. Zhao, G. Liu and W. Jin, *J. Membr. Sci.*, 2019, **579**, 210-218.

51.   J. Y. Lee, S. O. Hwang, H. J. Kim, D. Y. Hong, J. S. Lee and J. H. Lee, *Sep. Purif. Technol.*, 2019, **209**, 383-391.

52.   P. Y. Zheng, X. Q. Li, J. K. Wu, N. X. Wang, J. Li and Q. F. An, *J. Membr. Sci.*, 2018, **548**, 215-222.

53.   X. Wang, J. Chen, M. Fang, T. Wang, L. Yu and J. Li, *Sep. Purif. Technol.*, 2016, **163**,

39-47.

54. F. U. Nigiz and N. D. Hilmioglu, *J. Appl. Polym. Sci.*, 2017, **134**, 45211.

55. Y. Lan, P. Peng and P. Chen, *Adv. Polym. Tech.*, 2018, **37**, 3297-3304.

56. Y. Lan and P. Peng, *J. Appl. Polym. Sci.*, 2019, **136**, 46912.